How accurately should we model ice shelf melt rates?

How accurately should we model ice shelf melt rates?

D. N. Goldberg,[1]N. Gourmelen, [1]S. Kimura, [2]R. Millan [3], K. Snow [4]

[1]School of Geosciences, University of Edinburgh, Edinburgh, United Kingdom
[2]JAMSTEC, Japan
[3]U. California-Irvine, United States
[4]Australia National University, Canberra, Australia

Key Points:

- Satellite measurement of melt rates shows high spatial variability under two fast-flowing ice shelves
- Ice-sheet response to ice shelf melt depends on the pattern of melt rates as well as their spatial average
- The ability of an ocean model to reproduce this pattern depends on accurate bathymetry and ice shelf draft data

Abstract

Assessment of ocean-forced ice sheet loss requires that ocean models be able to represent sub-ice shelf melt rates. However, spatial accuracy of modelled melt is not well investigated, and neither is the level of accuracy required to assess ice sheet loss. Focusing on a fast-thinning region of West Antarctica, we calculate spatially resolved ice-shelf melt from satellite altimetry, and compare against results from an ocean model with varying representations of cavity geometry and ocean physics. Then, we use an ice-flow model to assess the impact of the results on grounded ice. We find that a number of factors influence model-data agreement of melt rates, with bathymetry being the leading factor; but this agreement is only important in isolated regions under the ice shelves, such as shear margins and grounding lines. To improve ice sheet forecasts, both modelling and observations of ice-ocean interactions must be improved in these critical regions.

1 Introduction

In certain locations along the Antarctic coastline [*Arneborg et al.*, 2012; *Dutrieux et al.*, 2014; *Greenbaum et al.*, 2015], warm Circumpolar Deep Water (CDW) exists on the continental shelf as a result of Ekman upwelling, weaker sea ice growth and deep oceanic troughs [*Jenkins et al.*, 2016; *Walker et al.*, 2013; *Petty et al.*, 2013], leading to high ice-shelf basal melt rates. In recent years, this melt has led to a large reduction in ice-shelf mass, particularly in the Amundsen Sea region [*Pritchard et al.*, 2012; *Paolo et al.*, 2015]. This reduction lessens buttressing of the ice sheet, increasing ice sheets' contribution to sea levels [*Thomas*, 1979; *Shepherd et al.*, 2004; *Jacobs et al.*, 2012; *Joughin et al.*, 2014].

Estimates of melt rates under Amundsen ice shelves have typically been area-averaged or area-integrated; either because estimates are based on hydrographic measurements [e.g., *Jacobs et al.*, 2011; *Rignot et al.*, 2013; *Randall-Goodwin et al.*, 2015; *Miles et al.*, 2016], or because the spacing of satellite altimetry tracks does not allow for spatially-resolved measurement [*Pritchard et al.*, 2012; *Paolo et al.*, 2015]. However, a number of studies have found spatially resolved measurements through high-resolution remote sensing methods [*Dutrieux et al.*, 2013; *Berger et al.*, 2017; *Gourmelen et al.*, 2017], showing that melt rates can differ widely from their areal average at spatial scales on the order of kilometers.

Meanwhile there has been a great deal of effort in the modelling of ice-ocean interactions in the Amundsen [e.g., *Payne et al.*, 2007; *Robertson*, 2013; *Dutrieux et al.*, 2014; *St-Laurent et al.*, 2015; *Kimura et al.*, 2017; *Nakayama et al.*, 2017]. While regional ocean models have been successful in reproducing ocean circulation and its link to bulk ice-shelf melt, ice modelling suggest that the *location* of ice removal from an ice shelf, in addition to its bulk value, may impact its buttressing capacity [*Goldberg et al.*, 2012; *Goldberg and Heimbach*, 2013; *Seroussi et al.*, 2017; *Arthern and Williams*, 2017]. The extent to which ocean models reproduce this spatial variability is unclear, and there is a need to strengthen the link between ocean and ice modelling if assessments of ice-sheet response to ocean forcing are to be made.

In this study, we employ a high-resolution ocean model with newly derived bathymetric data, validated against high-resolution satellite observations of melt, to better constrain the spatial variations in ice-shelf melt rates and evaluate their effect on ice-sheet stability using an adjoint-modelling approach. Focussing on Dotson and Crosson ice shelves, both situated in the Amundsen Sea and subject to strong CDW forcing, we examine the effects of different representations of bathymetry, ice-shelf draft, and physics of the ice-ocean boundary layer upon both melt rates and impact to grounded ice. We find that a number of factors are important to reproducing the observed spatial melt variability; but that capturing this variability is more important in some locations than others, at least where ice-sheet response is of interest.

2 Study Area

Smith, Pope, and Kohler Glaciers are three narrow interconnected ice streams in the Amundsen sector of West Antarctica, which drain into Crosson and Dotson Ice shelves. For purpose of discussion we adopt terminology from *Khazendar et al.* [2016] and *Gourmelen et al.* [2017] and refer to them (in east-to-west order) as Pope, Smith, Kohler East, and Kohler West (Fig. 3(a)). Although their contribution to ice flux from the continent is ∼7-8 times smaller than that of Thwaites and Pine Island Glaciers [*Shepherd et al.*, 2002], their observed thinning rates are even larger than that of these bigger ice streams [*McMillan et al.*, 2014a]. They have exhibited significant grounding line retreat in recent years, with the Smith grounding line retreating at rates upward of 2 km a^{-1} [*Scheuchl et al.*, 2016]. Ice-sheet modelling suggests that this retreat may have been induced by a decrease in buttressing from the Crosson and Dotson Ice Shelves [*Goldberg et al.*, 2015],

consistent with observations of increased velocities close to the grounding line of these ice streams [*Mouginot et al.*, 2014; *Lilien et al.*, 2018].

This drop in buttressing may be related to submarine melt-induced thinning, which can decrease buttressing [e.g., *Shepherd et al.*, 2004]. High melt rates have been observed for both Dotson and Crosson in recent years [*Depoorter et al.*, 2013; *Rignot et al.*, 2013; *Randall-Goodwin et al.*, 2015; *Miles et al.*, 2016; *Gourmelen et al.*, 2017; *Lilien et al.*, 2018]. Between 2003-2008, Dotson and Crosson had net average thinning rates of 3.1 and 6.5 m a^{-1}, respectively [*Rignot et al.*, 2013]; and both have had strong thinning trends for the last two decades [*Paolo et al.*, 2015].

Previously, numerical modelling of ice-ocean interactions under these ice shelves has been challenging due to inaccurate bathymetric information [*Schodlok et al.*, 2012]. A previous estimate of bathymetry, RTOPO [*Timmermann et al.*, 2010], was constructed from a series of bathymetric soundings. However, the dataset contains little information underneath Crosson and Dotson. A recent study [*Millan et al.*, 2017] used gravity data from Operation IceBridge to generate a far more detailed bathymetric map of the region, revealing a significant cavity beneath Crosson Ice Shelf as well as a substantial oceanographic connection between Crosson and Dotson. The findings raise questions of whether models require accurate bathymetry to assess oceanographic influence on ice sheets.

3 Methods

3.1 Melt rates from remote sensing

We generate swath elevation of Dotson and Crosson from CryoSat-2 between 2010 and 2015 [*Gourmelen et al.*, 2018] and, to avoid interference of advecting ice-shelf topography, solve for the Lagrangian rate of surface elevation change on a 500 by 500m grid [*Gourmelen et al.*, 2017]. The Lagrangian rate of change is performed using Sentinel-1 derived velocities [*McMillan et al.*, 2014b]. The melt rate is assessed through the following [*Jenkins and Doake*, 1991]:

$$m = \dot{a} - \frac{\dot{s} + s\nabla \cdot \boldsymbol{u}}{1 - \frac{\rho_i}{\rho_w}} \tag{1}$$

where m is basal melt rate, $\dot{a}$ is the surface mass balance [*van Wessem et al.*, 2016], ρ_i is ice density of 917 kg m^{-3}, ρ_w nominal ocean density of 1028 kg m^{-3}, $\boldsymbol{u}$ is ice velocity, and s is surface elevation from the DEM, corrected for a 1.5 m penetration bias.

3.2 Ocean cavity modelling

We use the Massachusetts Institute of Technology general circulation model (MITgcm; *Marshall et al.* [1997]) to model the circulation and melt rates underneath Dotson and Crosson Ice Shelves. The ocean model uses a stereographic polar projected grid and is restricted to a small domain (Fig. 1) which includes the ice-shelf cavities. External ocean boundary conditions are imposed from the output of a regional ocean simulation of the Amundsen Sea and shelf break [*Kimura et al.*, 2017]. The Kimura simulation was forced by atmospheric reanalysis and agrees well with available observations, and can be considered a reliable product for conditions at our domain boundaries. Monthly averages of temperature, salinity and velocity for 2010-2014 are interpolated to our domain boundaries. The model is spun-up for 2 years with 2010 forcing. No sea-ice or ocean surface forcing is included in the model.

Several different bathymetries and ice-shelf drafts are tested. We use RTOPO bathymetry and draft for comparison with the *Millan et al.* [2017] bathymetry and draft – referred to as the *Millan* bathymetry and draft. Additionally we use an ice-shelf draft calculated from the CryoSat-derived DEM for the period 2010-2015, assuming hydrostatic floatation and a uniform firn column air content of 17 m [*Ligtenberg et al.*, 2014] – referred to as the *CryoSat* draft. (We note that the Millan ice-shelf draft is derived from BEDMAP2 ice-shelf surface elevation [*Fretwell et al.*, 2013].)

Sub-ice shelf melt rates are calculated with a viscous sublayer model, which parameterizes turbulent fluxes of heat and salt just beneath the ice [*Losch*, 2008]. These fluxes are determined by turbulent exchange coefficients [*Holland and Jenkins*, 1999]. While some studies assume constant exchange coefficients [e.g., *Losch*, 2008; *Seroussi et al.*, 2017], MITgcm explicitly represents their dependency on near-ice velocities [*Dansereau et al.*, 2014]. We carry out simulations with both velocity-dependent and non-velocity dependent parameterizations. In the velocity-dependent runs, the frictional drag coefficient c_D in the formulation

$$u_*^2 = c_D|\boldsymbol{U}|^2 \tag{2}$$

(where u_*^2 is normalised interfacial drag, and $\boldsymbol{U}$ is near-ice velocity) is chosen to give area-average modelled melt similar to that of the observations for Dotson and Crosson. In the non-velocity dependent run, the temperature exchange coefficient (γ_T) is chosen to achieve the same (with γ_S, the salt exchange coefficient, held to a fixed ratio). Experiments are summarised in Table 1, and other relevant ocean model parameters are given in Table S1 of the Supplement.

3.3 Ice sheet-ice shelf modelling

We use the STREAMICE ice flow package of MITgcm [*Goldberg and Heimbach*, 2013] to model the response and sensitivity of Smith, Pope and Kohler Glaciers to melt rates under Dotson and Crosson. We use it as a standalone model, run in the domain indicated in Fig. 1(a) with 450 m resolution, and a fixed time step of $\frac{1}{24}$ years. BEDMAP2 data gives bathymetry and initial ice thickness.To address the lack of cavity data in BEDMAP2, we artificially deepen the bed by 50% seaward of its grounding line. While our modification of BEDMAP2 could bias against grounding line advance, the historic trend has been one of thinning and retreat. Still, this highlights the need for more reliable topographic data sets that extend over the entire continent.

In order to assess sensitivities the model is calibrated to observations, i.e. a model *inversion* is carried out. As described in the Section 2.2 of the Supplement, we constrain the time-evolving model, which is forced by ocean-modelled melt, to MEaSUREs (450 m) velocities [*Rignot et al.*, 2011] as well as a record of grounded thinning rates [*Gourmelen et al.*, 2018]. Basal traction and Glen's flow law coefficient [*Cuffey and Paterson*, 2010] are used as controls – as in *Goldberg et al.* [2015], grounded ice stiffness is determined by estimating the thermal steady-state, and Glen's law coefficient is adjusted only in floating ice.

The number of control parameters is roughly 2.5×10^5, so to minimize model-data misfit an adjoint approach is used [*MacAyeal*, 1992]. We use the Automatic Differentiation tool OpenAD [*Utke et al.*, 2008] which allows adjoint sensitivities of STREAMICE to be generated easily in both time-independent and time-dependent modes [*Goldberg et al.*, 2016].

Finally, calibrated parameters are used to initialise time-dependent model runs. The time-dependent adjoint model is used to assess sensitivity of grounded ice volume to melt rates over 15 years. We do not force our model with surface accumulation as we expect its low values in this region (30-40 cm per year, *Arthern et al.* [2006]) to have minimal dynamic impact over the time scale investigated; however, such forcing would be necessary for century-scale runs.

We stress that our use of thinning observations in our calibration is not meant to reproduce evolution of the system over a specific time window; rather, it is to initialise the model in a dynamic state representative of that of Smith, Pope and Kohler. The ice model, calibration and initialisation processes, and adjoint sensitivity calculation are explained in more detail in the Supplement [*Goldberg*, 2011; *Pattyn et al.*, 2013; *Fürst et al.*, 2015].

4 Results

4.1 Remotely-sensed melt rates

The 2011-2015 average surface elevation of Dotson and Crosson Ice Shelves is shown in Fig. 1. The surface depression related to the channel discussed in *Gourmelen et al.* [2017] is clearly visible, as is another smaller, narrower depression just to the west. Crosson Ice Shelf has a number of linear features in its surface, including a long narrow depression connecting the Smith grounding line to the tip of Bear Peninsula. This feature corresponds to a region of strong localised shear in the velocity field (Fig. 3(a)).

Melt rates derived from our calculation of surface rate-of-change and advective processes are shown in Fig. 2(a). Again, a clear signal of the channelised melting from *Gourmelen et al.* [2017] can be seen. Other high-melting regions are near the Smith and Pope grounding lines, as well as an elongated region south of Bear Peninsula, just east of the Dotson-Crosson shear margin. Thinning is evident in this region from the altimetry (Fig S1, Supplement).

The results suggest little melt in the south-east portion of Crosson and even localised freezing. Freezing is likely an artefact of our lagrangian tracking, since Crosson is heavily rifted in these regions, and freezing is unlikely given nearby observed ocean temperatures [*Randall-Goodwin et al.*, 2015; *Jenkins et al.*, 2018].

4.2 Modelled melt rates

Fig. 2(b-d) show melt rate results, averaged for each of the simulations over the years 2011-2015. Area-average melt rates (separately for each ice shelf and combined) are given in Table 1. For each model result, the average is over the region where there is circulation beneath an ice shelf. For the satellite-derived melt rates, two values are found: one in which rates are filtered between -100 ma^{-1} and +100 ma^{-1} (from examination of outliers in a melt-rate distribution), and one between 0 and +100 ma^{-1}. The latter value assumes that the negative melt rates found are artefacts, and the ocean melt-rate parameters c_D and γ_T are based on this value.

Both runs with the Millan bathymetry and velocity-dependent melt (Figs. 2(b,c)) show a channelised feature along the western margin of Dotson, similar to observations. However, melt is elevated along the entire margin, in contrast to observations. It is worth noting that elevated melt is indicated by the observations along the west margin, just upstream of the grounding line protrusion. Thus it is possible that these two "tributaries" of the channelised melt region are simply expressed in differing degrees by the model and observations.

Melt rates with the CryoSat draft (Figs. 2(c,d)) have a similar pattern to observations along the western margin of Crosson, just south of Bear Peninsula. Here the mixed layer is likely guided by inverted depressions in the ice shelf (Fig. S2, Supplement), while Coriolis focuses the outflow on the margin. In contrast, the topography of the Millan draft guides the flow northward (fig. 2(b)).

With a velocity-independent melt parameterisation (Fig. 2(d)), melt is actually decreased in the location of the channelised feature, and in Crosson's west shear margin, suggesting a velocity-driven mechanism in the channel. On the other hand, there is better agreement with observations near the Pope, Smith, and Kohler East grounding lines. (All models other than the RTOPO model indicate high melt near the Kohler West grounding line.) The low melt rates near the grounding line in the velocity-dependent models are due to low velocities just beneath the shelf. This is in line with idealised models using velocity-dependent melt rates [*Little et al.*, 2009; *Snow et al.*, 2017], which also suggest low melting at the grounding line. The RTOPO model (see Fig. S3, Supplement) does indicate elevated melt rates along Dotson's west margin, but the poor agreement in every other respect is likely due to the incorrect bathymetry.

The time series of melt shows a generally decreasing trend (Fig. S4, Supplement). This is in line with oceanographic estimates [*Jenkins et al.*, 2018], although a temporary increase in 2013 is seen. As our study focuses on melt rate patterns this is not detrimental to our aims, but care should be taken when interpreting our modelled melt rate evolution.

4.3 Grounded ice sensitivity to melt rates

Adjoint sensitivities of VAF (Volume Above Floatation; *Dupont and Alley* [2005]) to melt rates are calculated for Dotson and Crosson Ice Shelves (Fig. 3(b)). Specifically these are found with respect to a "control run" ($CONTROL$) forced with time-average melt from Model 1, so chosen due to the close correspondence between the Millan draft and the initial ice draft. VAF is used as it is a measure of potential contribution to sea levels; but it is not the only measure of melt rate impact on grounded ice, as discussed below.

Upon examining the adjoint sensitivities, some interesting patterns emerge. Sensitivities are seen to be small over most of Dotson, aside from the grounding line of Kohler West. Sensitivity is slightly elevated where channelised melt-driven thinning takes place, but this is still small. On Crosson, sensitivities are largest in the vicinity of ice rumples and along the Pope, Smith and Kohler East grounding lines. Of note, however, is the high sensitivity along the velocity shear margin of Crosson where it borders Dotson and the southern edge of Bear Peninsula. We note that the results are broadly similar to those of *Reese et al.* [2018], who examined instantaneous velocity response of a time-independent model to ice-shelf mass removal on a coarse grid.

The calculated adjoint sensitivities can be used to generate linearized responses of VAF to different melt rate perturbations as follows. If m_i is the melt rate in an ocean grid cell i, then the incremental VAF response (relative to that of the $CONTROL$ experiment) is found by

$$\Delta VAF = \sum_i (m_i - m_i^{ref}) \delta^* m_i, \tag{3}$$

i.e. a summation over all cells i, where m_i^{ref} is the melt rate from Model 1, and $\delta^* m_i$ is the sensitivity of ΔVAF to melt rate in the cell i:

$$\delta^* m_i = \frac{\partial(\Delta VAF)}{\partial m_i}, \tag{4}$$

evaluated at m^{ref}.

Eq. 3 is evaluated for each melt field (modelled and observed), with results given in Table 1. Despite the observed melt pattern having a smaller spatial average than that of Model 1, it yields a larger VAF loss. The reason can be traced to greater melt rates near grounding lines, particularly Kohler West and Kohler East. Still, the ice-sheet impact is relatively similar among the models (aside from the RTOPO model).

It is also informative to consider the melt rate pattern of "maximal impact" from a grounded ice loss perspective – this is a melt rate perturbation which is an exact scaling of melt rate sensitivities:

$$\Delta m_i^{max} = \left(\frac{nM}{\sum_i \delta^* m_i} \right) \delta^* m_i \tag{5}$$

where n is the total cell count, and M is a perturbation spatial average. Choosing M = 3 ma^{-1} (in line with the approximate thinning rate of both Crosson and Dotson over the past two decades, *Paolo et al.* [2015]) leads to a linearly predicted VAF loss of 32.1 km^3. For reference, a spatially uniform perturbation of 3 ma^{-1} yields predicted loss of 8.6 km^3.

The above are linear estimates – a limitation of the adjoint approach. For instance, grounding line retreat leads to loss of backstress from basal traction and can lead to increased grounding line thickness, which cannot be detected by linearising about a fixed trajectory. We run two additional time-dependent simulations of the same length as $CONTROL$: one in which melt rate is equal to (m^{ref}+Δm^{max}); and one in which it is equal to (m^{ref}+M). The former is referred to as the $FOCUS$ run below, while the latter is referred to as $CONST$. The impact of the perturbations on thinning and ice speed relative to $CONTROL$ are shown in Figs. 3(c-f). $FOCUS$ yields considerably higher grounded thinning of the ice streams (up to 70 m over the modelled period in some locations), and also increased grounded speeds (up to 220 ma^{-1}), as well as considerable speedup of Crosson. The associated VAF losses in the $FOCUS$ and $CONST$ experiments are 41.3 and 14.0 km^3 a^{-1}, respectively. These are higher than the predicted linear responses, likely due to model nonlinearities.

5 Discussion

In our experiments, the ocean simulation which gives the best agreement with observations in terms of reproducing large-scale features (Model 2) nonetheless underestimates melt in key areas such as grounding lines. The results raise questions as to the requirements of ocean cavity models to best predict future impacts of ocean forcing on Antarctica. If the most important aspect of the melt field is near the grounding line, then accurate bathymetry – which determines delivery of dense CDW – becomes crucial.

The importance of melt near the grounding line also highlights the importance of the ocean model's melt-rate parameterisation. Although our velocity-independent melt model reproduces the high melt rates observed near the grounding line, this does not necessarily mean such a parameterisation is the correct one to use, as it could neglect important processes, such as potential accelerated melt due to runoff [*Berger et al.*, 2017; *Smith et al.*, 2017], or potential ice-shelf collapse due to channelised melt [*Gourmelen et al.*, 2017]. Furthermore, we do not represent tidal effects, which could potentially be important [*Jourdain et al.*, 2019]. Moreover, our analysis assumes the satellite-inferred melt rates to be "truth", but the assumption of hydrostatic floatation could lead to systemic errors, particularly within ∼5 kilometers of the grounding line [*Brunt et al.*, 2010]. Thus, improved observations of melt rates in the vicinity of the grounding line are needed, as well as an improved representation of ocean physics in this critical region.

In our analysis, we have assumed submarine melting to be the primary driver of loss of grounded ice. However, there are other processes that can affect ice-shelf buttressing. Ice stiffness (the Glens law parameter) influences ice flow in a similar manner to thickness and ice-shelf weakening can have a similar effect to melt-induced thinning. In fact, *Lilien et al.* [2018] infer weakening of the Dotson-Crosson margin from 1996-2011. Adjoint sensitivity to Glen's law parameter (not shown) has a pattern similar to that of melting, and it is possible that observed speedup of Smith, Pope and Kohler East is due to weakening in this shear margin. Alternatively, thinning in the western shear margin of Crosson could potentially be influencing and accelerating this weakening: as an ice shelf thins in its shear margin, shear stress and strain rates increase. Larger shearing stresses might then lead to higher levels of ice damage [*Borstad et al.*, 2016], and thus further weakening. If such a process were to continue indefinitely, it could lead to an effective separation of Crosson and Dotson ice shelves, as has been observed for Thwaites Ice Tonge

and Thwaites Eastern Ice Shelf – an event which has led to a large shift in the grounded velocity of Thwaites Glacier [*Mouginot et al.*, 2014].

The *FOCUS* ice model experiment leads to far more thinning and speedup than the *CONST* run. Still, the additional mass loss, $\sim$3 km^3 a^{-1}, is not large relative to the $\sim$21 km^3 a^{-1} currently being lost from the region. Moreover there is little modelled grounding line retreat, despite extensive retreat observed [*Rignot et al.*, 2014]. The lack of grounding line retreat (which would lead to additional *VAF* loss) may be because the nature of the experiments precludes melt under newly floating ice; other modelling studies [*Seroussi et al.*, 2017; *Arthern and Williams*, 2017] suggest that melting of newly exposed shelf near the grounding line has a large impact on retreat. Additionally, the initial model ice thickness could be predisposed against retreat: BEDMAP thicknesses are much higher than initial thickness used in *Goldberg et al.* [2015] along most of the grounding line (Fig. S7, Supplement). That study produced large grounding line retreat using the same model at the same resolution. Thus our experiments show that melt pattern – and not just melt volume – can have an important impact on grounded ice; but other processes are required for extensive retreat.

6 Conclusions

By comparing high-resolution satellite-inferred observations of ice-shelf melt against ocean cavity models, we have shown that reasonable agreement can be achieved with sufficiently accurate boundary conditions such as ice-shelf draft and ocean bathymetry. However, analysis of sensitivities of an ice sheet-ice shelf model suggests this agreement may only be important in certain locations, if the aim is to model and understand ice-sheet response to ocean forcing. Equivalently, melt rate patterns can be as important as bulk melt in determining grounded ice response to melt.

For small, narrow ice shelves like Crosson and Dotson, these locations of high sensitivity to melt are likely to include those near the grounding lines and regions of high shear. Thus it is very important that ocean models represent ice-ocean physics accurately in these critical locations. Moreover, it is important that observations of melt in these critical locations be improved – since without this, the veracity of ocean models in these locations, and hence their utility in predicting future ice-sheet response to climate variability and change, cannot be assessed.

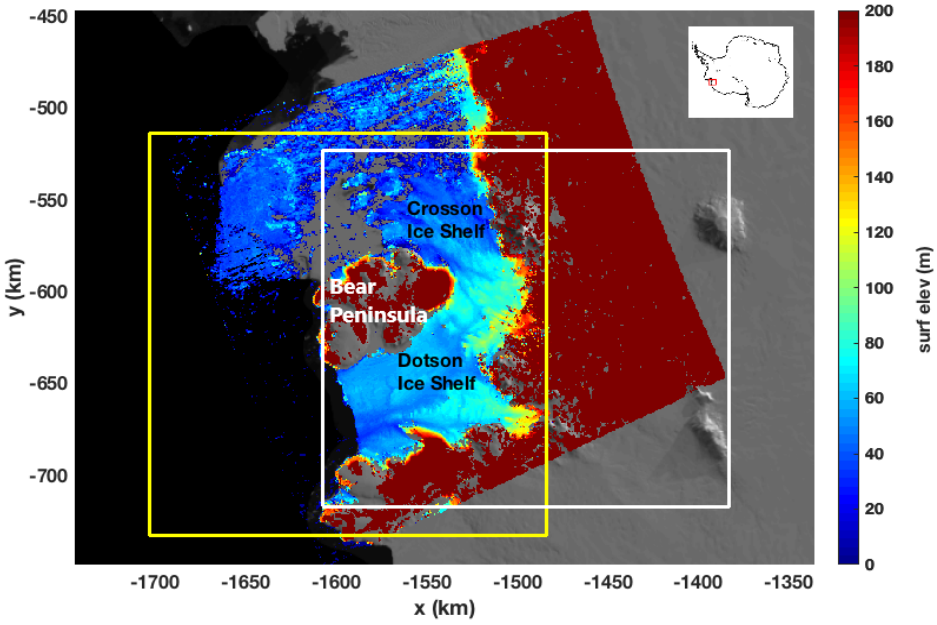

Figure 1. Average surface elevation of Dotson and Crosson Ice Shelves, 2011-2015, from CryoSat observations (shading), overlain on MOA imagery. The yellow box indicates the domain of the ocean model used in our study, and the white box that of our ice model. Coordinates are in terms of the stereopolar projection centered at 71°S.

In this work, we have utilised an adjoint model to investigate melt sensitivities. Despite its being a linear approximation of nonlinear processes, we would advocate such an approach in future investigations of ocean forcing of ice sheets, as it can identify locations where understanding of ice-ocean processes is crucial.

Acknowledgments

This work was supported by Natural Environment Resources Council grant NE/M003590/1. The code used to generate all results, as well as documentation of the models used, is available at mitgcm.org. All cryosat data is available from ftp://science-pds.cryosat.esa.int. Ice and ocean modelling output used to produce figures are available as Supplementary Material. Additionally DNG is grateful to J DeRydt for helpful conversations in the development of this work.

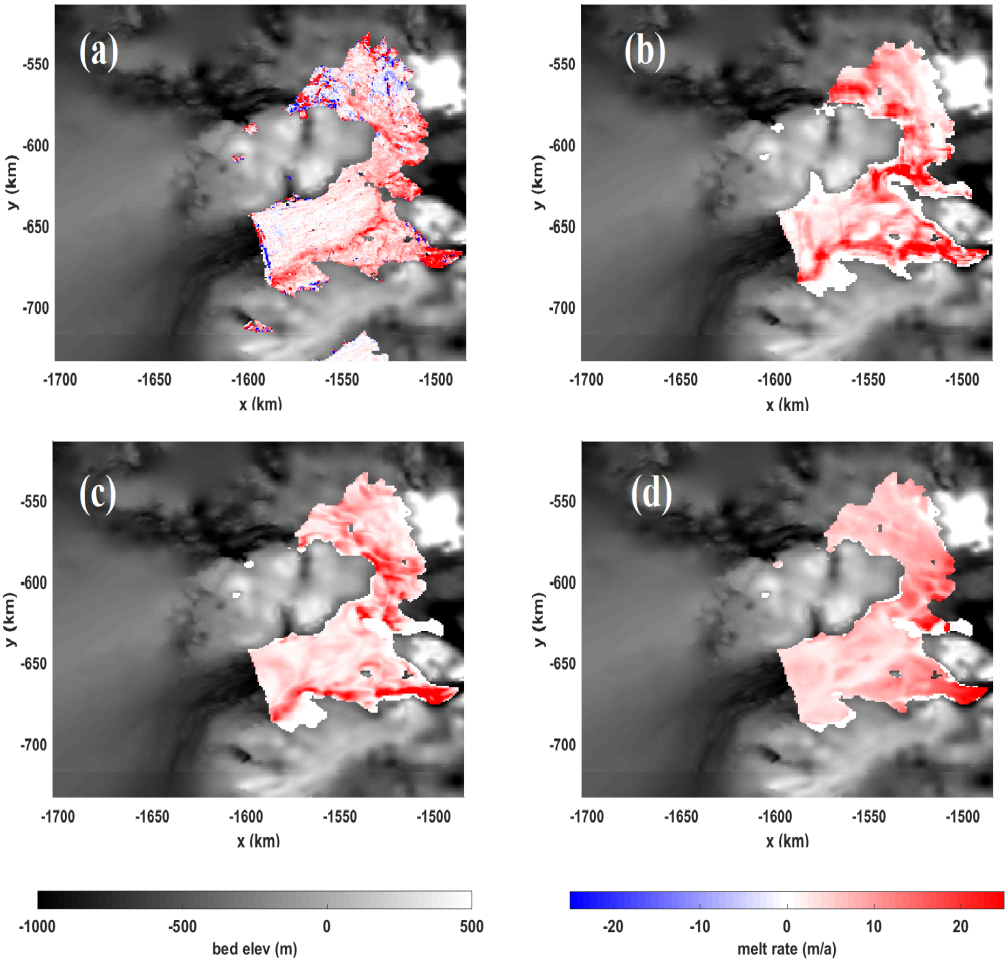

Figure 2. (a) Melt rates inferred from CryoSat elevation change using Eq. 1 (color shading), overlain on the Millan bathymetry (B/W) and plotted for the ocean model domain. The Millan dataset does not reach the edge of the domain in the west, and so is replaced by BEDMAP2 in this region. (b) Average melt rate of Model 1 over the same period. (c) Similarly for Model 2. (d) Similarly for Model 3.

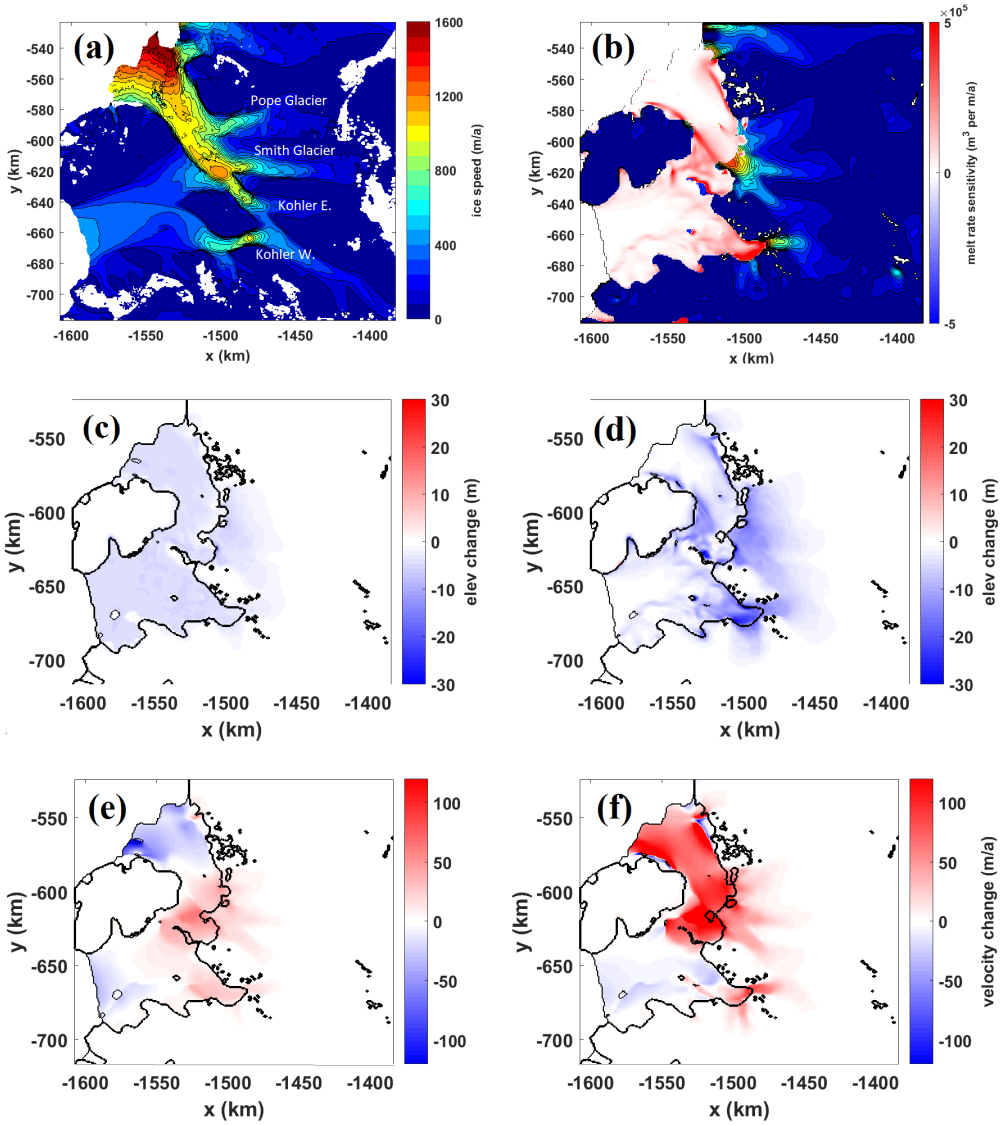

Figure 3. (a) MEaSUREs ice speed within ice model domain. (b) Adjoint melt rate sensitivities over the ice shelf (Red/Blue shading) and modelled grounded ice velocity (filled contours). (c) Total modelled surface elevation change in $CONST$ ice model simulation, relative to that of $CONTROL$. Note the grounding line location is given by the thick black contour. (d) As in (c) but for $FOCUS$ simulation. (e) Change in ice-stream and ice-shelf speed in $CONST$ simulation relative to to $CONTROL$. Again, the grounding line is denoted by the thick black contour. Difference in velocity is projected onto the direction of velocity in $CONTROL$. (f) as in (e) but for $FOCUS$ simulation.

(Obs / model)	**Bathy**	**Draft**	**Melt Param.**	**Avg Melt, Crosson (ma^{-1})**	**Avg Melt, Dotson (ma^{-1})**	**Avg Melt, Combined (ma^{-1})**	**Est. VAF Loss (km^3)**
CryoSat	N/A	N/A	N/A	7.15 (5.39)	6.68 (5.70)	6.86 (5.58)	2.4 (-4.0)
Model 1	Millan	Millan	u-dep	7.11	7.80	7.55	N/A
Model 2	Millan	CryoSat	u-dep	6.72	6.43	6.53	-4.2
Model 3	Millan	CryoSat	u-indep	7.42	6.82	7.05	-3.0
Model 4	RTOPO	RTOPO	u-dep	N/A	2.66	2.66	-23

Table 1. Table of observed and modelled melt rates and grounded volume response. Melt values in parentheses indicate an alternative method of filtering the observations. The final column represents a linear estimate of VAF loss relative to the *CONTROL* run, calculated via Eq. 3.

manuscript submitted to *Geophysical Research Letters*

References

Arneborg, L., A. K. Wåhlin, G. Björk, B. Liljebladh, and A. H. Orsi, Persistent inflow of warm water onto the central amundsen shelf, *Nature Geoscience*, *5*, 876–880, doi:10.1038/ngeo1644, 2012.

Arthern, R., and C. R. Williams, The sensitivity of west antarctica to the submarine melting feedback, *Geophysical Research Letters*, *44*(5), 2352–2359, doi:10.1002/2017GL072514, 2017.

Arthern, R. J., D. P. Winebrenner, and D. G. Vaughan, Antarctic snow accumulation mapped using polarization of 4.3-cm wavelength microwave emission, *Journal of Geophysical Research: Atmospheres*, *111*(D6), D06,107, doi:10.1029/2004JD005667, 2006.

Berger, S., R. Drews, V. Helm, S. Sun, and F. Pattyn, Detecting high spatial variability of ice shelf basal mass balance, roi baudouin ice shelf, antarctica, *The Cryosphere*, *11*(6), 2675–2690, doi:10.5194/tc-11-2675-2017, 2017.

Borstad, C., A. Khazendar, B. Scheuchl, M. Morlighem, E. Larour, and E. Rignot, A constitutive framework for predicting weakening and reduced buttressing of ice shelves based on observations of the progressive deterioration of the remnant Larsen B Ice Shelf, *Geophysical Research Letters*, *43*(5), 2027–2035, doi:10.1002/2015GL067365, 2016.

Brunt, K. M., H. A. Fricker, L. Padman, T. A. Scambos, and S. O?Neel, Mapping the grounding zone of the ross ice shelf, antarctica, using icesat laser altimetry, *Annals of Glaciology*, *51*(55), 71?79, doi:10.3189/172756410791392790, 2010.

Cuffey, K., and W. S. B. Paterson, *The Physics of Glaciers*, 4th ed., Butterworth Heinemann, Oxford, 2010.

Dansereau, V., P. Heimbach, and M. Losch, Simulation of subice shelf melt rates in a general circulation model: Velocity-dependent transfer and the role of friction, *Journal of Geophysical Research: Oceans*, *119*(3), 1765–1790, doi:10.1002/2013JC008846, 2014.

Depoorter, M. A., J. L. Bamber, J. A. Griggs, J. T. M. Lenaerts, S. R. M. Ligtenberg, M. R. van den Broeke, and G. Moholdt, Calving fluxes and basal melt rates of Antarctic ice shelves, *Nature*, *502*, 89–92, doi:doi:10.1038/nature12567, 2013.

Dupont, T. K., and R. Alley, Assessment of the importance of ice-shelf buttressing to ice-sheet flow, *Geophys. Res. Lett.*, *32*, L04,503, 2005.

Dutrieux, P., D. G. Vaughan, H. F. J. Corr, A. Jenkins, P. R. Holland, I. Joughin, and A. H. Fleming, Pine island glacier ice shelf melt distributed at kilometre scales, *The Cryosphere*, *7*(5), 1543–1555, doi:10.5194/tc-7-1543-2013, 2013.

Dutrieux, P., et al., Strong sensitivity of pine island ice-shelf melting to climatic variability, *Science*, *343*(6167), 174–178, doi:10.1126/science.1244341, 2014.

Fretwell, P., et al., Bedmap2: improved ice bed, surface and thickness datasets for Antarctica, *The Cryosphere*, *7*(1), 375–393, doi:10.5194/tc-7-375-2013, 2013.

Fürst, J. J., G. Durand, F. Gillet-Chaulet, N. Merino, L. Tavard, J. Mouginot, N. Gourmelen, and O. Gagliardini, Assimilation of antarctic velocity observations provides evidence for uncharted pinning points, *The Cryosphere*, *9*(4), 1427–1443, doi:10.5194/tc-9-1427-2015, 2015.

Goldberg, D. N., A variationally-derived, depth-integrated approximation to a higher-order glaciologial flow model, *Journal of Glaciology*, *57*, 157–170, 2011.

Goldberg, D. N., and P. Heimbach, Parameter and state estimation with a time-dependent adjoint marine ice sheet model, *The Cryosphere*, *7*(6), 1659–1678, doi:10.5194/tc-7-1659-2013, 2013.

Goldberg, D. N., C. M. Little, O. V. Sergienko, A. Gnanadesikan, R. Hallberg, and M. Oppenheimer, Investigation of land ice-ocean interaction with a fully coupled ice-ocean model, Part 2: Sensitivity to external forcings, *Journal of Geophysical Research-Earth Surface*, *117*, F02,038, doi:10.1029/2011JF002246, 2012.

Goldberg, D. N., P. Heimbach, I. Joughin, and B. Smith, Committed retreat of smith, pope, and kohler glaciers over the next 30 years inferred by transient model calibration, *The Cryosphere*, *9*(6), 2429–2446, doi:10.5194/tc-9-2429-2015, 2015.

Goldberg, D. N., S. H. K. Narayanan, L. Hascoet, and J. Utke, An optimized treatment for algorithmic differentiation of an important glaciological fixed-point problem, *Geoscientific Model Development*, *9*(5), 1891–1904, doi:10.5194/gmd-9-1891-2016, 2016.

Gourmelen, N., M. Escorihuela, A. Shepherd, L. Foresta, A. Muir, A. Garcia-Mondjar, M. Roca, S. Baker, and M. Drinkwater, Cryosat-2 swath interferometric altimetry for mapping ice elevation and elevation change, *Advances in Space Research*, *62*(6), 1226 – 1242, doi:https://doi.org/10.1016/j.asr.2017.11.014, 2018.

Gourmelen, N., et al., Channelized melting drives thinning under a rapidly melting antarctic ice shelf, *Geophysical Research Letters*, *44*(19), 9796–9804, doi:

10.1002/2017GL074929, 2017.

Greenbaum, J. S., et al., Ocean access to a cavity beneath Totten Glacier in East Antarctica, *Nature Geoscience*, *8*, 294–298, doi:https://doi.org/10.1038/ngeo2388, 2015.

Holland, D. M., and A. Jenkins, Modelling thermodynamic ice-ocean interactions at the base of an ice shelf, *J. Phys. Ocean.*, *29*, 1787–1800, doi:https://doi.org/10.1175/1520-0485(1999)029, 1999.

Jacobs, S., A. Jenkins, H. Hellmer, C. Guilivi, F. Nitsche, B. Huber, and R. Guerrero, The Amundsen Sea and the Antarctic Ice Sheet, *Oceanography*, *25*, doi:https://doi.org/10.5670/oceanog.2012.90, 2012.

Jacobs, S. S., A. Jenkins, C. Giulivi, and P. Dutrieux, Stronger ocean circulation and increased melting under Pine Island Glacier ice shelf, *Nat. Geosci.*, doi:10.1038/NGEO1188, 2011.

Jenkins, A., and C. Doake, Ice?ocean interaction on Ronne Ice Shelf, Antarctica, *Journal of Geophysical Research: Oceans*, *96*(C1), 791–813, doi:10.1029/90JC01952, 1991.

Jenkins, A., P. Dutrieux, S. Jacobs, E. J. Steig, H. Gudmundsson, J. Smith, and K. Heywood, Decadal ocean forcing and antarctic ice sheet response: Lessons from the amundsen sea, *Oceanography*, *29*, doi:https://doi.org/10.5670/oceanog.2016.103, 2016.

Jenkins, A., D. Shoosmith, P. Dutrieux, S. Jacobs, T. W. Kim, S. H. Le, H. K. Ha, and S. Stammerjohn, West antarctic ice sheet retreat in the amundsen sea driven by decadal oceanic variability, *Nat. Geoscience*, *11*, 733?738, doi:https://doi.org/10.1038/s41561-018-0207-4DO, 2018.

Joughin, I., B. E. Smith, and B. Medley, Marine ice sheet collapse potentially under way for the Thwaites Glacier Basin, West Antarctica, *Science*, *344*(6185), 735–738, doi:10.1126/science.1249055, 2014.

Jourdain, N. C., J.-M. Molines, J. L. Sommer, P. Mathiot, J. Chanut, C. de Lavergne, and G. Madec, Simulating or prescribing the influence of tides on the amundsen sea ice shelves, *Ocean Modelling*, *133*, 44 – 55, doi:https://doi.org/10.1016/j.ocemod.2018.11.001, 2019.

Khazendar, A., E. Rignot, D. Schroeder, H. Seroussi, M. Schodlok, B. Scheuchl, J. Mouginot, T. Sutterley, and I. Velicogna, Rapid submarine ice melting in the

grounding zones of ice shelves in West Antarctica, *Nature Communications*, *7*, 13,243, doi:http://dx.doi.org/10.1038/ncomms13243, 2016.

Kimura, S., et al., Oceanographic controls on the variability of ice?shelf basal melting and circulation of glacial meltwater in the amundsen sea embayment, antarctica, *Journal of Geophysical Research: Oceans*, *122*(12), 10,131–10,155, doi:10.1002/2017JC012926, 2017.

Ligtenberg, S. R. M., P. Kuipers Munneke, and M. R. van den Broeke, Present and future variations in antarctic firn air content, *The Cryosphere*, *8*(5), 1711–1723, doi:10.5194/tc-8-1711-2014, 2014.

Lilien, D. A., I. Joughin, B. Smith, and D. E. Shean, Changes in flow of crosson and dotson ice shelves, west antarctica, in response to elevated melt, *The Cryosphere*, *12*(4), 1415–1431, doi:10.5194/tc-12-1415-2018, 2018.

Little, C. M., A. Gnanadesikan, and M. Oppenheimer, How ice shelf morphology controls basal melting, *Journal of Geophysical Research*, *114*, C12,007, 2009.

Losch, M., Modeling ice shelf cavities in a z coordinate ocean general circulation model, *Journal of Geophysical Research: Oceans*, *113*(C8), n/a–n/a, doi:10.1029/2007JC004368, 2008.

MacAyeal, D. R., The basal stress distribution of Ice Stream E, Antarctica, inferred by control methods, *Journal of Geophysical Research*, *97*, 595–603, 1992.

Marshall, J., C. Hill, L. Perelman, and A. Adcroft, Hydrostatic, quasi-hydrostatic, and nonhydrostatic ocean modeling, *Journal of Geophysical Research: Oceans*, *102*(C3), 5733–5752, doi:10.1029/96JC02776, 1997.

McMillan, M., A. Shepherd, A. Sundal, K. Briggs, A. Muir, A. Ridout, A. Hogg, and D. Wingham, Increased ice losses from Antarctica detected by CryoSat-2, *Geophysical Research Letters*, *41*(11), 3899–3905, doi:10.1002/2014GL060111, 2014a.

McMillan, M., et al., Rapid dynamic activation of a marine-based arctic ice cap, *Geophysical Research Letters*, *41*(24), 8902–8909, doi:10.1002/2014GL062255, 2014b.

Miles, T., S. H. Lee, A. Wåhlin, H. K. Ha, T. W. Kim, K. M. Assmann, and O. Schofield, Glider observations of the Dotson Ice Shelf outflow, *Deep Sea Research Part II: Topical Studies in Oceanography*, *123*, 16 – 29, doi:https://doi.org/10.1016/j.dsr2.2015.08.008, 2016.

Millan, R., E. Rignot, V. Bernier, M. Morlighem, and P. Dutrieux, Bathymetry of the Amundsen Sea Embayment sector of West Antarctica from Operation IceBridge gravity and other data, *Geophysical Research Letters*, *44*(3), 1360–1368, doi:10.1002/2016GL072071, 2017.

Mouginot, J., E. Rignot, and B. Scheuchl, Sustained increase in ice discharge from the amundsen sea embayment, west antarctica, from 1973 to 2013, *Geophysical Research Letters*, *41*(5), 1576–1584, doi:10.1002/2013GL059069, 2014.

Nakayama, Y., D. Menemenlis, M. Schodlok, and E. Rignot, Amundsen and bellingshausen seas simulation with optimized ocean, sea ice, and thermodynamic ice shelf model parameters, *Journal of Geophysical Research: Oceans*, *122*(8), 6180–6195, doi:10.1002/2016JC012538, 2017.

Paolo, F. S., H. A. Fricker, and L. Padman, Volume loss from Antarctic ice shelves is accelerating, *Science*, *348*(6232), 327–331, doi:10.1126/science.aaa0940, 2015.

Pattyn, F., et al., Grounding-line migration in plan-view marine ice-sheet models: results of the ice2sea mismip3d intercomparison, *Journal of Glaciology*, *59*(215), 410?422, doi:10.3189/2013JoG12J129, 2013.

Payne, A. J., P. R. Holland, A. Shepherd, I. C. Rutt, A. Jenkins, and I. Joughin, Numerical modeling of ocean-ice interactions under Pine Island Bay's ice shelf, *Journal of Geophysical Research-Oceans*, *112*, C10,019, 2007.

Petty, A. A., D. L. Feltham, and P. R. Holland, Impact of Atmospheric Forcing on Antarctic Continental Shelf Water Masses, *Journal of Physical Oceanography*, *43*(5), 920–940, doi:10.1175/JPO-D-12-0172.1, 2013.

Pritchard, H. D., S. R. M. Ligtenberg, H. A. Fricker, D. G. Vaughan, M. R. van den Broeke, and L. Padman, Antarctic ice-sheet loss driven by basal melting of ice shelves, *Nature*, *484*, 502–505, doi:doi:10.1038/nature10968, 2012.

Randall-Goodwin, E., et al., Freshwater distributions and water mass structure in the Amundsen Sea Polynya region, Antarctica, *Elementa*, *5*, 65, doi:http://doi.org/10.12952/journal.elementa.000065, 2015.

Reese, R., G. H. Gudmundsson, A. Levermann, and R. Winkelmann, The far reach of ice-shelf thinning in antarctica, *Nature Climate Change*, *8*, 53–57, doi:https://doi.org/10.1038/s41558-017-0020-x, 2018.

Rignot, E., J. Mouginot, and B. Scheuchl, Ice flow of the Antarctic Ice Sheet, *Science*, *333*(6048), 1427–1430, doi:10.1126/science.1208336, 2011.

Rignot, E., S. Jacobs, J. Mouginot, and B. Scheuchl, Ice-Shelf Melting Around Antarctica, *Science*, *341*(6143), 266–270, doi:10.1126/science.1235798, 2013.

Rignot, E., J. Mouginot, M. Morlighem, H. Seroussi, and B. Scheuchl, Widespread, rapid grounding line retreat of Pine Island, Thwaites, Smith and Kohler glaciers, West Antarctica from 1992 to 2011, *Geophysical Research Letters*, *41*, 3502–3509, doi:10.1002/2014GL060140, 2014.

Robertson, R., Tidally induced increases in melting of Amundsen Sea ice shelves, *Journal of Geophysical Research: Oceans*, *118*(6), 3138–3145, doi:10.1002/jgrc.20236, 2013.

Scheuchl, B., J. Mouginot, E. Rignot, M. Morlighem, and A. Khazendar, Grounding line retreat of Pope, Smith, and Kohler Glaciers, West Antarctica, measured with Sentinel-1a radar interferometry data, *Geophysical Research Letters*, *43*(16), 8572–8579, doi:10.1002/2016GL069287, 2016.

Schodlok, M. P., D. Menemenlis, E. Rignot, and M. Studinger, Sensitivity of the ice-shelf/ocean system to the sub-ice-shelf cavity shape measured by nasa icebridge in pine island glacier, west antarctica, *Annals of Glaciology*, *53*(60), 156?162, doi:10.3189/2012AoG60A073, 2012.

Seroussi, H., Y. Nakayama, E. Larour, D. Menemenlis, M. Morlighem, E. Rignot, and A. Khazendar, Continued retreat of thwaites glacier, west antarctica, controlled by bed topography and ocean circulation, *Geophysical Research Letters*, pp. n/a–n/a, doi:10.1002/2017GL072910, 2017.

Shepherd, A., D. J. Wingham, and J. Mansley, Inland thinning of the Amundsen Sea sector, West Antarctica, *Geophys. Res. Lett.*, *29*, L1364, doi:10.1029/2001GL014183, 2002.

Shepherd, A., D. J. Wingham, and E. Rignot, Warm ocean is eroding West Antarctic Ice Sheet, *Geophys. Res. Lett.*, *31*, L23,402, 2004.

Smith, B. E., N. Gourmelen, A. Huth, and I. Joughin, Connected subglacial lake drainage beneath thwaites glacier, west antarctica, *The Cryosphere*, *11*(1), 451–467, doi:10.5194/tc-11-451-2017, 2017.

Snow, K., D. N. Goldberg, P. R. Holland, J. R. Jordan, R. J. Arthern, and A. Jenkins, The response of ice sheets to climate variability, *Geophysical Research Letters*, *44*(23), 11,878–11,885, doi:10.1002/2017GL075745, 2017.

549 St-Laurent, P., J. M. Klinck, and M. S. Dinniman, Impact of local winter cooling
550 on the melt of Pine Island Glacier, Antarctica, *Journal of Geophysical Research:*
551 *Oceans*, *120*(10), 6718–6732, doi:10.1002/2015JC010709, 2015.
552 Thomas, R. H., The dynamics of marine ice sheets, *Journal of Glaciology*, *24*, 167–
553 177, 1979.
554 Timmermann, R., et al., A consistent data set of antarctic ice sheet topography, cav-
555 ity geometry, and global bathymetry, *Earth System Science Data*, *2*(2), 261–273,
556 doi:10.5194/essd-2-261-2010, 2010.
557 Utke, J., U. Naumann, M. Fagan, N. Tallent, M. Strout, P. Heimbach, C. Hill,
558 D. Ozyurt, and C. Wunsch, OpenAD/F: A modular open source tool for au-
559 tomatic differentiation of Fortran codes, *ACM Transactions on Mathematical*
560 *Software*, *34*, 2008.
561 van Wessem, J. M., et al., The modelled surface mass balance of the antarctic
562 peninsula at 5.5 km horizontal resolution, *The Cryosphere*, *10*(1), 271–285, doi:
563 10.5194/tc-10-271-2016, 2016.
564 Walker, D. P., A. Jenkins, K. Assmann, D. Shoosmith, and M. Brandon, Oceano-
565 graphic observations at the shelf break of the Amundsen Sea, Antarctica, *Journal*
566 *of Geophysical Research: Oceans*, *118*(6), 2906–2918, doi:10.1002/jgrc.20212, 2013.